JOURNAL OF SPACECRAFT AND ROCKETS
Vol. 35, No. 5, September–October 1998

Review and Extension of Computational Methods for Noncircular Cross-Sectional Weapons

F. G. Moore, R. M. McInville, and T. C. Hymer
U.S. Naval Surface Warfare Center, Dahlgren, Virginia 22448-5000

A review of current state-of-the-art methods for computing aerodynamics of noncircular cross-sectional weapon concepts has been performed. In addition, an improved engineering method has been developed to compute aerodynamics of these nonaxisymmetric body configurations. The improved method is based on extending current state-of-the-art methods for computing aerodynamics of noncircular wing–body shapes based on circular wing–body methods. Specific additions to the state-of-the-art methods currently in use include extensions to a broader class of cross-sectional bodies and to a higher angle of attack; extensions to allow improved accuracy at low crossflow Mach number and to allow body cross-sectional shape to impact the critical crossflow Reynolds number; and a method to treat wing–body interference factor corrections as a function of body geometry, Mach number, and angle of attack. The new methods were applied to a broad class of noncircular body alone and wing–body configurations for which wind-tunnel data were available. In general, results for normal force, axial force, and center-of-pressure predictions were quite good for a semiempirical methodology, over the Mach number and angle-of-attack range where data were available. Range of variables included Mach numbers as low as 0.3 and as high as 14 and angles of attack to 60 deg.

Nomenclature

A_C = cross-sectional area of circular cylinder, ft^2
A_{eq} = cross-sectional area of circular cylinder equal to that of body with noncircular cross section
AR = wing or tail aspect ratio
A_{ref} = reference area (maximum cross-sectional area of body, if a body is present, or planform area of wing if wing alone), ft^2
$A(x)$ = body cross-sectional area as a function of position along body axis, ft^2

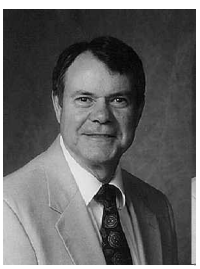

Frank G. Moore was employed at the U.S. Naval Surface Warfare Center (NSWC) in 1963 as a cooperative engineering student. He completed his B.S., M.S., and Ph.D. degrees in aerospace engineering from Virginia Polytechnic Institute and State University in 1967, 1968, and 1971, respectively. He has had a wide variety of experience at NSWC, including that of researcher, project manager, line manager of several different branches, program manager, and, more recently, staff scientist. He has published extensively in the open literature and given many invited lectures and talks both in the United States and internationally. His most noteworthy contributions have been in the development of semiempirical aerodynamic prediction methods. He is an Associate Fellow of AIAA.

Roy M. McInville attended North Carolina State University in Raleigh, majoring in aerospace engineering and earning B.S., M.S., and Ph.D. degrees. During this period, he participated in the cooperative education program at NASA Wallops Island and the graduate student research program at NASA Langley Research Center, as well as serving as the supervisor of an environmental testing laboratory for five years. He came to the U.S. Naval Surface Warfare Center (NSWC), Dahlgren Division, in 1984 and has been involved with NSWC aeroprediction code developmental work for the past six years.

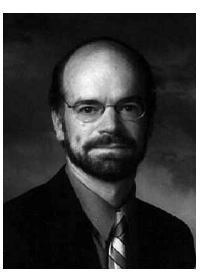

Thomas C. Hymer received a B.S. degree in aerospace engineering from the Pennsylvania State University in May 1985. Since then, he has been employed at the U.S. Naval Surface Warfare Center (NSWC) in the Aeromechanics Branch. He has been involved with flight dynamics and 6DOF simulations, in addition to working on the NSWC Aeroprediction Code.

Received Dec. 30, 1997; revision received June 30, 1998; accepted for publication July 13, 1998.

a, b = semimajor and semiminor axis, respectively, of ellipse
a' = body shape parameter[30]
C_A = axial force coefficient
$(C_A)_{\alpha=0}$ = axial force coefficient at 0-deg angle of attack
C_D = drag coefficient
C_d, C_{dC} = local and total crossflow drag coefficients
$(C_{dC})_1, (C_{dC})_2$ = subcritical and supercritical value, respectively, of C_{dC}
C_L = lift coefficient
C_M = pitching moment coefficient
$C_{M_L}, C_{M_{NL}}$ = linear and nonlinear components, respectively, of pitching moment coefficient
C_N = total normal force coefficient
C_{N_B} = normal force coefficient of the body
$C_{N_L}, C_{N_{NL}}$ = linear and nonlinear components, respectively, of the normal force coefficient
$C_{N_{T(V)}}$ = normal force coefficient on tail due to wing-shed vortices
$(C_{N_\alpha})_W, (C_{N_\alpha})_T$ = normal force coefficient slope of wing and tail, respectively
$(C_n/C_{n_0})_{SB}, (C_n/C_{n_0})_N$ = ratio of the local normal force coefficient of a body with a noncircular cross section to that with a circular cross section calculated by slender body and Newtonian theory, respectively
d, d_B = diameter of body and base diameter of body, respectively
F = ratio of wing–body interference factor of a noncircular cross-sectional configuration to that of a circular cross-sectional configuration
K = ratio of lifting surface normal force coefficient in the presence of a body to that of the lifting surface alone at $\delta = 0$ deg
$K_{B(W)}, K_{B(T)}$ = ratio of additional body normal force coefficient in the presence of a wing or tail to that of the wing or tail alone at $\delta = 0$ deg
$K_{W(B)}, K_{T(B)}$ = ratio of wing or tail normal force coefficient in the presence of a body to that of the wing or tail alone at $\delta = 0$ deg
k = parameter used to define corner radius for squares and triangles, r_n/W_M
$k_{B(W)}, k_{B(T)}$ = ratio of additional body normal force coefficient due to the presence of a deflected wing or tail to that of the wing or tail alone at $\alpha = 0$ deg
$k_{W(B)}, k_{T(B)}$ = ratio of normal force contribution of a deflected wing or tail in the presence of a body to that of the wing or tail alone at $\alpha = 0$ deg
l = total body length
l_{ref} = reference length, which is body diameter
l_1, l_2, l_3, l_i = individual segments of body length where body has variable noncircular cross section
M = Mach number
M_N, V_N = Mach number and velocity normal to body
NF = Newtonian correction factor
NF_1 = Newtonian correction factor for an ellipse at $\alpha \geq 20$ deg
R_N = Reynolds number
R_{N_C} = Reynolds number where flow transitions from subcritical to supercritical conditions
r = local body radius, ft
r_{eq}, d_{eq} = radius and diameter, respectively, of a circular cross-sectional body that has the same cross-sectional area as that of the noncircular cross-sectional body
r_n = corner radius of a rounded corner on square or triangle
s = radius of body plus wing or tail semispan
W = length of one side of a triangle or square
W_m = maximum width of a triangle or square as measured normal to the velocity vector
x = distance along body axis, ft
x_{CP} = center of pressure measured about some reference location
x_m = reference location about which center of pressure is measured
α = angle of attack, rad or deg
δ = deflection angle of control surface, rad, deg
η = parameter used in viscous crossflow theory for nonlinear body normal force (in this context, it is the ratio of the normal force of a circular cylinder of given length-to-diameter ratio to that of a cylinder of infinite length)
λ = taper ratio of fin, C_t/C_r
Φ = roll position of missile [$\Phi = 0$ deg corresponds to fins in the plus (+) orientation] and the leeward plane; $\Phi = 45$ deg corresponds to fins rolled to the cross (×) orientation

Subscripts

C = circular body
NC = noncircular body
∞ = freestream conditions

I. Introduction

THE desire to increase weapon range and maneuverability, to design weapons that are more optimum from an aircraft total drag and radar signature standpoint, or to provide optimum loadout of multiple missiles in a ship's vertical launcher has driven weapons designers to consider nonaxisymmetric body shapes. Some typical shapes of interest are shown in Fig. 1. Although most missiles in

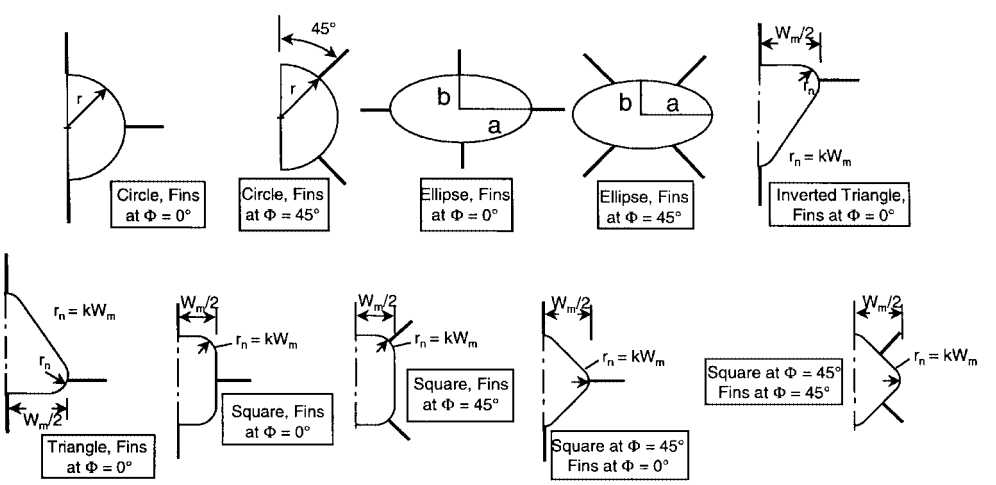

Fig. 1 Some noncircular cross-sectional, wing–body configurations of interest.

existence today in the United States and other countries have axisymmetric body configurations, these conceptual design tradeoffs of various configurations other than axisymmetric require engineering estimates of aerodynamics. Current state-of-the-art methods for predicting aerodynamics of nonaxisymmetric body shapes with engineering accuracy are much more limited than for axisymmetric bodies. The more limited methodology for nonaxisymmetric bodies compared with axisymmetric bodies is primarily driven by the fact that to get reasonable accuracy of the aerodynamics requires an accurate description of the body geometry. To describe the geometry of a complex body shape accurately can take days or weeks depending on the requirements of the aerodynamics code being used.

The present approaches to computing aerodynamics fall into two basic classes. The first class requires the description of the body geometry in some detail for aerodynamic computations. Methods that fall into this class[1–4] have various levels of sophistication and likewise various levels of accuracy. They vary from engineering methods[1] to full Navier–Stokes computations.[4]

The second class of codes for calculating aerodynamics of a nonaxisymmetric body is based on an equivalent axisymmetric body. The beauty of this approach is the fact that an existing axisymmetric body code can be used to calculate nonaxisymmetric body aerodynamics if the area distribution of the body is known. The area distribution requires a lot less time to define than a detailed configuration geometry. On the other hand, one should anticipate possibly larger errors in predicting the aerodynamics than an approach where the detailed geometry is required. The ease of use, fast turnaround, and lower cost may be worth the reduced accuracy, however. This type of approach was pioneered by the methods of Whitcomb[5] and Jorgensen.[6–10]

The Missile DATCOM[11] code uses the method of Jorgensen to estimate aerodynamics of elliptic cross-sectional shapes to any angle of attack (AOA) and other cross-sectional shapes at small AOA. However, no such code is available for other than elliptical cross-sectional shapes at high AOA. There are several areas where the Jorgensen approach needs improvement. First, the method was derived on the basis of slender body theory (SBT) for low AOA and modified Newtonian theory (MNT) at higher AOA. The MNT, strictly speaking, is accurate only for higher Mach numbers and therefore needs to be corrected for lower Mach numbers. Second, most of the data available for making these empirical corrections to MNT are at low speed, and thus additional data or computational fluid dynamics efforts are needed for higher Mach number. Third, the Jorgensen correlation factors based on SBT and MNT work reasonably well in predicting normal forces for elliptical configurations but not so well for triangular and square cross-sectional bodies. Fourth, the Jorgensen approach uses SBT for interference between the wings and bodies with no nonlinear corrections for AOA, Mach number, or wing shape. The Missile Datcom[11] improves upon this problem by the use of the equivalent AOA method.[12] This allows the nonlinear corrections of wing–body lift to be included and extends the AOA boundary to 20–25 deg for interference effects. Finally, no corrections are included in the Jorgensen method for the axial force wave component of drag for the noncircular bodies compared with the circular bodies.

Although the Jorgensen method has its shortcomings, it is still the method most compatible with the U.S. Naval Surface Warfare Center aeroprediction code (APC)[13] because the APC is currently developed for axisymmetric bodies. The goal of the present work is therefore to modify the work of Jorgensen to improve upon the shortcomings stated previously. If this work is successful, a more robust, more accurate, yet simple code for computing aerodynamics of nonaxisymmetric body missile configurations will be available. This publication presents the summary results of this new technology. For details of the work, the reader is referred to Ref. 14.

II. Analysis

The goal of the present work is to extend the APC[13] to include simple nonaxisymmetric body configurations. As discussed in the Introduction, the approach most compatible with the axisymmetric body techniques of Ref. 13 is one that computes the aerodynamics of a nonaxisymmetric body on the basis of an equivalent axisymmetric body. The most developed of these approaches is that of Jorgensen.[6–10] As such, it is instructive to review the Jorgensen[6–10] method briefly, to point out the weak areas discussed in the Introduction, and then to address the present improved methodology to overcome these shortcomings.

A. Review of Jorgensen's Method

Jorgensen's method[6–10] for the static aerodynamics of a body alone is given by

$$C_A = (C_A)_{\alpha=0}\cos^2\alpha \tag{1}$$

$$C_N = \frac{\sin(2\alpha)\cos(\alpha/2)}{A_{\text{ref}}}\int_0^l \left(\frac{C_n}{C_{n_0}}\right)_{\text{SB}}\left(\frac{\mathrm{d}A}{\mathrm{d}x}\right)\mathrm{d}x + \frac{2\eta C_{d_C}\sin^2\alpha}{A_{\text{ref}}}\int_0^l \left(\frac{C_n}{C_{n_0}}\right)_N r\,\mathrm{d}x \tag{2}$$

$$C_M = \frac{\sin(2\alpha)\cos(\alpha/2)}{A_{\text{ref}}l_{\text{ref}}}\int_0^l \left(\frac{C_n}{C_{n_0}}\right)_{\text{SB}}\frac{\mathrm{d}A}{\mathrm{d}x}(x_m - x)\,\mathrm{d}x + \frac{2\eta C_{d_C}\sin^2\alpha}{A_{\text{ref}}l_{\text{ref}}}\int_0^l \left(\frac{C_n}{C_{n_0}}\right)_N r(x_m - x)\,\mathrm{d}x \tag{3}$$

$$x_{\text{CP}}/l_{\text{ref}} = -(C_M/C_N) + (x_m/l_{\text{ref}}) \tag{4}$$

Equations (2) and (3) allow for continually varying cross sections along the body. Equation (1) is an assumed approximation for correlating axial force with AOA. It also requires a calculation of, or that experimental data be available for, axial force coefficient at zero AOA. Equations (2) and (3) both include the factors $(C_n/C_{n_0})_{\text{SB}}$ and $(C_n/C_{n_0})_N$. These factors represent the slender body (SB) and Newtonian approximations to the local normal force coefficient per unit length of the desired cross-sectional shape (C_n) to the similar coefficient for the equivalent circular cross-sectional shape (C_{n_0}). The radius of the equivalent cross-sectional shape is determined by

$$r_{\text{eq}} = \sqrt{A(x)/\pi} \tag{5}$$

where $A(x)$ represents the area of the nonaxisymmetric body as it varies along the body x axis. The first terms of both Eqs. (2) and (3) are the terms due to potential flow, and the second terms are those due to the viscous crossflow. Because SBT is applicable only for small AOAs, the coefficient $(C_n/C_{n_0})_{\text{SB}}$ can only be used for the first term of Eqs. (2) and (3). On the other hand, Newtonian impact theory is applicable at any AOA and can therefore be used for the second term of Eqs. (2) and (3). The term C_{d_C} is the crossflow drag coefficient for the equivalent body of revolution. Finally, both Eqs. (3) and (4) are defined about some reference point x_m. The terms $(C_n/C_{n_0})_{\text{SB}}$ and $(C_n/C_{n_0})_N$ are given in Ref. 6 for several ellipses. The term $(C_n/C_{n_0})_N$ is also given for some squares. Reference 11 gives the SB theory values of $(C_n/C_{n_0})_{\text{SB}}$ for several configurations.

When one reviews Eqs. (1–5), it is appropriate to specifically point out the weak points suggested in the Introduction. First, Eq. (1) assumes $(C_A)_{\alpha=0}$ of the equivalent axisymmetric body is the same as that for the noncircular body and that C_A varies as $\cos^2\alpha$ with AOA. These assumptions need further investigation. Second, $(C_n/C_{n_0})_N$ is accurate primarily at high Mach numbers. A correction for lower crossflow Mach numbers is probably required ($M_N < 2.0$) for accurate prediction of static aerodynamics at all AOAs and M_∞. Third, additional analytical equations need to be derived for $(C_n/C_{n_0})_N$ for other than elliptical cross-sectional shapes. This is required to expand the approach of Ref. 6 to a broader range of cross sections. Fourth, although Jorgensen discusses the impact of crossflow drag coefficient as a function of Reynolds number, he does not offer any methodology to correct for the sudden decrease in the crossflow

drag coefficient for Reynolds numbers above the critical value as a function of body cross-sectional shape. Finally, configuration aerodynamics need to be defined in such a way as to allow the interference terms between the wing and body to include nonlinearities. Reference 13 already has these nonlinearities included for circular bodies. This methodology has been validated to high AOA and for a large range of Mach numbers and configurations. However, this methodology also needs to be adjusted for the noncircular bodies being considered.

The remainder of the analysis section will take each of the problems discussed and briefly define the modifications or new methods necessary to attempt to achieve a more accurate and robust way of treating noncircular bodies than is available in either Ref. 6 or Ref. 11. The reader is referred to Ref. 14 for more elaboration and discussion of the new methods.

B. Body Alone Axial Force Approach

The axial force coefficient at zero AOA is composed of three components that arise from the wave drag generated by the flow as it is compressed on the body surface, the friction of the air as it passes over the body, and the pressure on the afterbody or base caused by the separation of the flow from the body surface.

For the present work, the base and wave drag are computed by using an equivalent axisymmetric body composed of a cross-sectional area equal to that of the nonaxisymmetric body. The skin-friction drag is computed by multiplying the skin-friction drag of the equivalent axisymmetric body by the ratio of the circumference of the nonaxisymmetric cross section to that of the equivalent axisymmetric cross section.

The method of Ref. 15 will be assumed for AOA changes in C_A, and Ref. 13 will be used for fin values of C_A. Hence, to compute C_A, we first determine the equivalent axisymmetric body. The axial force is computed as currently done in the AP95 (Ref. 13) code for this equivalent axisymmetric body with or without fins. The body alone value of C_A is then adjusted for the appropriate noncircular shape, and the fin values of C_A are held constant. The term C_A at AOA is then adjusted according to Ref. 15.

C. Values of $(C_n/C_{n_0})_{SB}$ and $(C_n/C_{n_0})_N$

When one applies Eqs. (2) and (3) to noncircular bodies, values of the parameters $(C_n/C_{n_0})_{SB}$ and $(C_n/C_{n_0})_N$ are required for the particular noncircular shape of interest. The term C_{dC} of these equations remains the crossflow drag coefficient of a circular cylinder with the radius defined by Eq. (5). Values of these parameters for ellipses using both SBT and MNT are given in Ref. 6 and shown here in Fig. 2 for convenience.

Values of $(C_n/C_{n_0})_N$ were not available for many other cases of interest. As a result, Ref. 14 derives this parameter for several cases of interest, including squares and triangles with various corner radii. Reference 11 contained approximate values of the slender body apparent mass parameters that allowed computation of $(C_n/C_{n_0})_{SB}$ for squares and triangles with no corner radius. These values were then allowed to go to 1 in a linear fashion when k goes to 0.5. Values of $(C_n/C_{n_0})_N$ and $(C_n/C_{n_0})_{SB}$ are given in Figs. 3 and 4 for the square and triangular cross sections, respectively, as a function of the corner radius parameter k. Figures 2–4 are used at any Mach number. However, the use of Newtonian theory at lower supersonic and subsonic Mach numbers will be discussed in the next section.

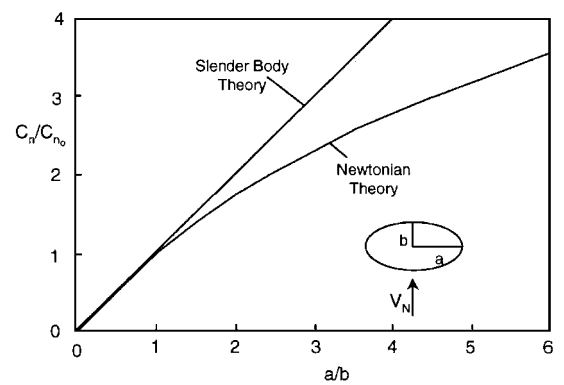

Fig. 2 Ratio of local normal force coefficient for an elliptic cross section to that for the equivalent circular cross section.

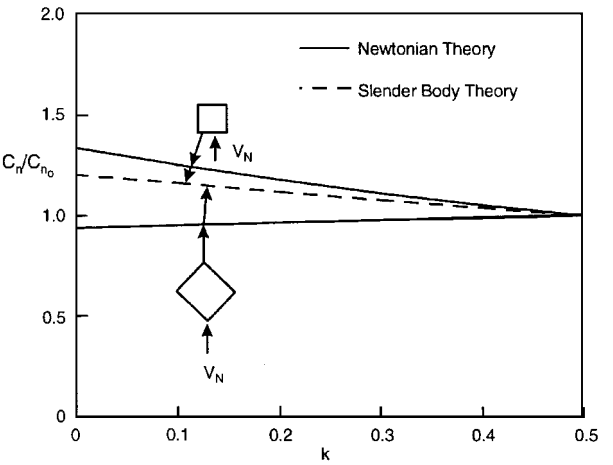

Fig. 3 Ratio of local normal force coefficient for a square cross section to that for the equivalent circular cross section.

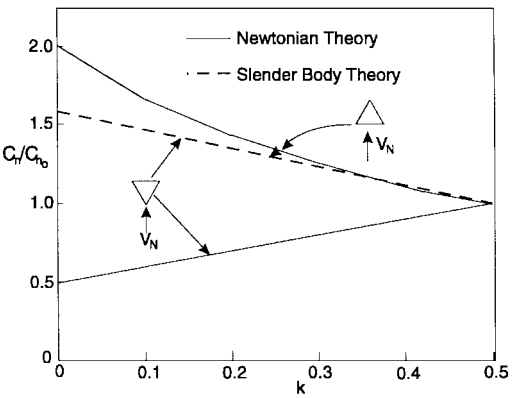

Fig. 4 Ratio of local normal force coefficient for a triangular cross section to that for the equivalent circular cross section.

It is interesting to note from Figs. 3 and 4 that SBT gives constant values of $(C_n/C_{n_0})_{SB}$ for both the triangle and square[11] independent of their orientation. On the other hand, Newtonian theory values of $(C_n/C_{n_0})_N$ vary depending on the orientation of the triangle or square. Newtonian impact theory is a function of the sine of the angle between the velocity vector and a tangent to the body surface to the second power. As a result, the configuration that has the base of the triangle normal to the flow has a fairly high value of the parameter $(C_n/C_{n_0})_N$, whereas the value when the triangle is inverted is about one-fourth of the larger value when the corner is sharp ($k = 0$). On the other hand, Ref. 11 shows the apparent mass to be independent of orientation of the triangle and square, and so a value of SBT is obtained for the parameter $(C_n/C_{n_0})_{SB}$ that is independent of orientation and is between the two values computed by Newtonian theory for both the square and triangle.

D. Newtonian Correction Factor

Figures 3 and 4 address one of the weak areas in the methodology of Refs. 6 and 11 discussed previously. A second problem that needs to be addressed is to provide a correction as a function of Mach number for the Newtonian theory curves of Figs. 2–4. Because the slender body curves are used at low AOA, and values of normal force are small, it is not as critical that these curves be corrected for nonslender bodies. On the other hand, the Newtonian theory curves are used at high AOA and could potentially be erroneous at lower Mach numbers.

Equations (2) and (3) for the body alone normal force and pitching moment will therefore be rewritten to include the factor NF, which represents the correction in the modified Newtonian values

of $(C_n/C_{n0})_N$ due to the crossflow Mach number not being infinite. Thus,

$$C_N = C_{N_L}\left(C_n/C_{n0}\right)_{\mathrm{SB}} + C_{N_{\mathrm{NL}}}\left(C_n/C_{n0}\right)_N \mathrm{NF} \tag{6}$$

$$C_M = C_{M_L}\left(C_n/C_{n0}\right)_{\mathrm{SB}} + C_{M_{\mathrm{NL}}}\left(C_n/C_{n0}\right)_N \mathrm{NF} \tag{7}$$

Both Eqs. (6) and (7) are based on body aerodynamics of a circle of equivalent cross-sectional area to that of the noncircular body cross section.

To compute NF, we will use available experimental data to compare $(C_n/C_{n0})_N$ of Figs. 2–4. If values of these parameters are not available directly, then the parameter NF can be approximated by comparing total force and moment data from tests to that predicted by Ref. 13 when NF is 1. The factor NF can then be computed to bring the theory more in line with experimental data. For this phase of the work we used Refs. 6, 7, and 16–23.

A brief explanation of why the factor NF is needed is in order. Basically, Newtonian impact theory assumes that all of the normal momentum of an air particle is lost upon direct impact on a body surface. The theory is derived based on very high Mach numbers, and past comparisons with experiment have shown the simple theory does indeed give quite accurate pressure information on simple body shapes as Mach number becomes large and the particle impact angle is near normal to the surface. As a consequence of the momentum of each air particle being deposited on a surface upon impact, the pressure coefficient on all areas that the flow does not see directly (shadowed regions), or leeward plane areas, is zero. This Newtonian assumption becomes increasingly erroneous as the Mach number decreases. Although the ratio $(C_n/C_{n0})_N$ tends to mitigate the error somewhat, due to the fact the error occurs on both the circular and noncircular configurations, it is logical to assume that the error is configuration dependent. If Eqs. (6) and (7) were applied only for crossflow Mach numbers greater than about 2–5, one could probably neglect the factor NF and still achieve reasonable accuracy for engineering codes. However, because most tactical weapons fly in the range of freestream Mach numbers less than 6, it is very important to have the factor NF defined.

The first noncircular configuration is the elliptical cross section of Fig. 2. This configuration has the most experimental data available and therefore is the easiest to define the factor NF. Results for elliptical configurations with $a/b = 0.5$, 2.0, and 3.0 are given in Fig. 5. Figure 5 was derived primarily from the data of Jorgensen[6,7] and Shereda et al.[23] in conjunction with the AP95 (Ref. 13). As a result of the combined usage of data and a code, some of the factor NF in Fig. 5 could be from errors in the AP95 itself. However, as seen in Fig. 5, if the errors are from the AP95, they are fairly consistent in terms of a general trend as a function of a/b.

Figure 5 was derived for AOAs greater than 20 deg because this is the region where one obtains the largest amount of separation in the leeward plane of the vehicle and therefore the region where Newtonian theory is least accurate. To blend in the factor $(\mathrm{NF})_1$ with

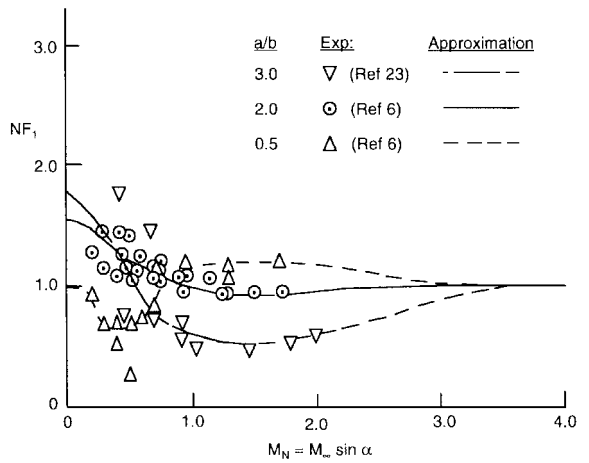

Fig. 5 Newtonian correction factor for an elliptical cross section ($\alpha \geq 20$ deg).

AOA, we assume a linear variation between AOA of 0 and 20 deg. That is,

$$\begin{aligned} \mathrm{NF} &= 1 + [(\mathrm{NF})_1 - 1](\alpha/20), \qquad \alpha \leq 20 \\ \mathrm{NF} &= (\mathrm{NF})_1, \qquad \alpha > 20 \end{aligned} \tag{8}$$

It was found that the approach of Eq. (8) was more accurate than the application of Fig. 5 fully at AOAs of less than 20 deg.

Several points are worthy of note in Fig. 5. First, for values of $a/b < 2.0$, NF_1 is close to 1 at crossflow Mach numbers of 2.0 and higher. Second, at low crossflow Mach numbers, the $a/b = 2.0$ and 3.0 configurations generate a large amount of nonlinear normal force compared with a circle. This is partly explained by Ref. 24. Reference 24 shows that the drag coefficients of various flat shapes coalesce at high Mach number but vary widely at low Mach numbers. The ellipse approaches a flat surface as a/b gets large. Third, the configuration for $a/b = 0.5$ appears to indicate a region of supercritical crossflow Reynolds number around $M_N = 0.5$ where the factor NF_1 decreases below 1. However, for $a/b = 0.5$, the value of NF more closely resembles Newtonian theory (NF is closer to 1) than the larger values of a/b when M_N is less than about 0.8. Finally, to estimate the effects of elliptical shapes other than $a/b = 0.5$, 2.0, or 3.0, a linear assumption is made that the factor varies between 1.0 for $a/b = 1.0$ and its value in Fig. 5 for a/b other than 1.

Values of the parameter NF for both square and triangular cross-sectional shapes are defined in Ref. 14 in a similar manner to that of the elliptical cross-sectional shapes. For the sake of brevity, these results are not shown here. Results for NF are defined[14] as a function of corner radius and crossflow Mach number for the square and triangular shapes. Suffice it to say that the factor NF can vary significantly from 1 for crossflow Mach numbers less than about 2.0. Hence, to assume NF is 1 can result in substantial errors in estimating body alone normal force at high AOA for many noncircular cross-sectional shapes.

E. Reynolds Number Effect on Crossflow Drag Coefficient

Because the methodology for computing the aerodynamics of nonaxisymmetric bodies is based on computing the aerodynamics of an equivalent axisymmetric body, the question arises as to whether a relationship can be derived for critical crossflow Reynolds numbers as a function of body cross-sectional shape. References 19 and 25 both give values of C_{d_C} as a function of crossflow Reynolds number and body cross-sectional shape for M_N values near zero.

Reference 19 correlated crossflow drag coefficient to a parameter $(R_N k^{1.3})$. For squares at $\Phi = 0$, it appears that the critical value of this parameter based on Ref. 19 can be defined as a function of k.

Thus for squares at $\Phi = 0$ deg,

$$\frac{R_{N_C}}{\left(R_{N_C}\right)_{k=0.5}} = \frac{0.083 + 1.36k - 1.44k^2}{k^{1.31}}, \qquad 0.02 \leq k \leq 0.5 \tag{9}$$

For the value of $k \leq 0.02$, a value of 0.02 could be used in Eq. (9). If the square is rotated to $\Phi = 45$ deg (diamond), then a better approximation to the data of Ref. 19 is

$$\frac{R_{N_C}}{\left(R_{N_C}\right)_{k=0.5}} = \frac{6.33k - 24.1k^2 + 26.1k^3}{k^{1.31}}, \qquad 0.02 \leq k \leq 0.5 \tag{10}$$

For ellipses, an approximation to the data of Ref. 17 is

$$\frac{R_{N_C}}{\left(R_{N_C}\right)_{a/b=1.0}} = \left(\frac{a}{b}\right)^{1.5} \tag{11}$$

Finally, for triangular shapes with the base normal to the flow, the correlation equation for the square at $\Phi = 0$ deg, Eq. (9), appears to correlate the data of Ref. 26 reasonably well. Likewise, when the flow is in the direction of the triangular tip or inverted triangle where the base is to the rear, the equation for the square rotated 45 deg, Eq. (10), appears acceptable.

Physically, what Eqs. (9–11) are saying is that, when the configuration has corners or approaches a flat plate in the direction normal to the velocity vector, the critical value of the crossflow Reynolds number increases. The amount of this increase is proportional to the sharpness of the corners or to the elongation of the body (ellipse). The increase in the critical crossflow Reynolds number for ellipses with increasing values of a/b or triangles and squares with decreasing values of k means that the mechanism that causes the drag bucket for circular cylinders is harder to establish itself for most noncircular cross sections. This drag bucket is caused by the reattachment of the boundary layer on the rear of a circular cylinder for supercritical Reynolds numbers.

F. Wing–Body Interference Effects

Jorgensen[6] used a combination of two approaches for the wing–body aerodynamics. The first approach was to simply use Newtonian theory to approximate $(C_n/C_{n_0})_N$ of Eqs. (2) and (3) for wing–body configurations where the body was noncircular and the wing was a simple extension of this. He then used a modified version of Ref. 27 to compute the slender body or linear theory term of Eqs. (1) and (2). As shown in Ref. 6, this approach significantly overpredicted the normal force while giving reasonable results for center of pressure. The primary reason for this overprediction of normal force was the failure to account for the nonlinearities that occur in the wing–body interference factor as AOA increases.

Missile DATCOM[11] improved upon the Jorgensen[6] approach by using the equivalent AOA method[12] to incorporate nonlinearities in the wing–body interference factor. This increased the AOA capability to 20–30 deg. On the other hand, Ref. 11 did not include triangles and squares for high AOA because Newtonian theory was not developed for those shapes. Also, the Newtonian correction factor for lower Mach number was not available. Reference 11 also did not include the Newtonian correction factor for all Mach numbers for ellipses.

References 13 and 28 developed a new approach for incorporating nonlinearities in the wing–body and body–wing interference factors. In this approach, each interference term was divided into a linear and a nonlinear component. The linear term was estimated by linear theory or SBT and the nonlinear term was estimated directly through the use of large missile component wind-tunnel databases. For regions where data were not available, the method was extrapolated based on engineering judgment and comparison with aerodynamics on various other missile aerodynamic databases. The net result of this approach was average accuracy levels at roll positions of 0 and 45 deg of ±10% on normal and axial force and ±4% of body length on center of pressure to AOAs of 90 deg. Exceptions to this accuracy were at low Mach number and high AOA where wind-tunnel data were in question and at high Mach number and AOA for a configuration with two sets of lifting surfaces where internal shock interactions became important.

As a result, the improved approach for incorporating nonlinearities into the wing–body interference factors of Refs. 13 and 28 will be the methods used here for noncircular bodies. The overall normal force coefficient equation for any wing–body–tail configuration can be written as follows:

$$C_N = C_{N_B} + \left\{\left[K_{W(B)} + K_{B(W)}\right]\alpha + \left[k_{W(B)} + k_{B(W)}\right]\delta_W\right\}\left(C_{N_\alpha}\right)_W + \left\{\left[K_{T(B)} + K_{B(T)}\right]\alpha + \left[k_{T(B)} + k_{B(T)}\right]\delta_T\right\}\left(C_{N_\alpha}\right)_T + C_{N_{T(V)}} \tag{12}$$

The first term in Eq. (12) is the normal force of the body alone including the linear and nonlinear components; the second term is the contribution of the wing (or canard) including interference effects and control deflection; the third term is the contribution of the tail including interference effects and control deflection; and the last term is the negative downwash effect on the tail resulting from wing-shed or body-shed vortices. The uppercase K represents the interference of the configuration with respect to AOA, and the lowercase k represents the interference with respect to control deflection. The subscripts $W(B)$ and $T(B)$ represent the change (or interference effect) of the wing and tail in the presence of the body, whereas the subscripts $B(W)$ and $B(T)$ indicate the additional lift (or interference effect) on the body because of the presence of wings or tails. When Eq. (12) was originally defined, it was associated with the linear aerodynamics only.[27] References 13 and 28 defined a linear and a nonlinear component of each of the terms in Eq. (12). The body alone term for noncircular bodies is defined by Eq. (7). The interference terms are all defined in the general form

$$K = \underset{\text{SBT}}{K_{\text{LT}}} + \Delta K(M, AR, \lambda, \Phi, \alpha) \tag{13}$$

The first term on the right-hand side is known from linear theory or SBT for circular cylinder configurations. The second term is computed empirically based on databases and is defined in terms of tables as a function of the variables M, AR, λ, Φ, and α in Refs. 13 and 28. These tables are all based on circular bodies however. The wing alone term is estimated by a fourth-order equation in AOA that is a function of Mach number and wing planform parameters. Finally, the last term in Eq. (12) is estimated based on slender body theory and nonlinearities incorporated through comparison to data. Once again, Refs. 13 and 28 summarize all of the nonlinear methods used in computing normal force, pitching moment, and center of pressure for axisymmetric body missile configurations.

Figure 1 gives a qualitative pictorial view of the configurations for which aerodynamics are desired. It is believed this set of configurations can be made broad enough to encompass most tactical weapons of interest to the community at large. It includes the circles of various diameter, ellipses of various eccentricity, and triangles and squares of various orientation as well as corner radius. To complement the body geometry, wings have been included at both the $\Phi = 0$ and 45 deg roll orientations on all configurations except the triangular shape (where wings were limited to the $\Phi = 0$ deg roll orientation only). The question that now must be addressed is how Eq. (13) will vary for the noncircular wing–body configurations of Fig. 1.

Fortunately, Nelson,[29] Est and Nelson,[30] and Sigal[31] have performed work on $K_{W(B)}$, $K_{B(W)}$, and $k_{W(B)}$ for low AOAs for noncircular configurations. Nelson[29] and Est and Nelson[30] defined the low AOA values of $K_{W(B)}$ for elliptical, square, and triangular cross-sectional shapes at moderate supersonic Mach numbers using an Euler code in conjunction with low-Mach-number experimental data. Because the equivalent AOA method used SBT for $K_{B(W)}$, no equivalent data for noncircular cross sections were given in Refs. 29 and 30 for this parameter. Figure 6 gives the wing–body interference term for elliptical cross-sectional shapes after being divided by that of the circular cross section near $\alpha = 0$ deg. This figure was derived from the data of Ref. 29 in conjunction with the circular body results of Ref. 27. The results of Ref. 29 were given as a function of a'/s_1,

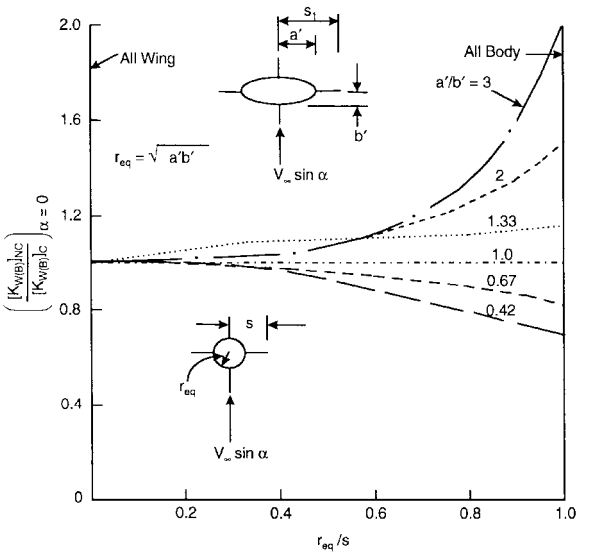

Fig. 6 Ratio of wing–body interference of an elliptical body to that of an equivalent circular body.[29]

and so they had to be translated to equivalent circular values through the relationship

$$\frac{r_{\text{eq}}}{s} = \frac{a'}{s_1}\left[\frac{1}{a'/s_1\left(1-\sqrt{C_1}\right)+\sqrt{C_1}}\right] \tag{14}$$

where $C_1 = a'/b'$. See Fig. 6 for the nomenclature.

It is interesting to note from Fig. 6 that, for most practical missile configurations where r_{eq}/s typically varies from about 0.1 to 0.7 and a/b is generally greater than 0.5 but less than 2.0, the noncircular $K_{W(B)}$ deviates from the circular value by, at most, 18% and for most cases less than that.

Reference 30 also showed that for the conditions investigated $k_{W(B)}$ varied only slightly from SBT for any of the cross-sectional shapes. As a result, the current nonlinear models in Refs. 13 and 28 will be used directly for this term.

As a first approximation, the body–wing interference term will be assumed to vary from its circular cylinder values in a proportional manner to the wing–body carryover. That is, if one defines

$$F = \frac{\left[K_{W(B)}\right]_{\text{NC},\alpha}}{\left[K_{W(B)}\right]_{C,\alpha}} \tag{15}$$

then

$$\left[K_{B(W)}\right]_{\text{NC},\alpha} = F\left[K_{B(W)}\right]_{C,\alpha} \tag{16}$$

$$\left[k_{B(W)}\right]_{\text{NC},\alpha} = F\left[k_{B(W)}\right]_{C,\alpha} \tag{17}$$

Also, as already mentioned,

$$\left[k_{W(B)}\right]_{\text{NC},\alpha} = \left[k_{W(B)}\right]_{C,\alpha} \tag{18}$$

It should be emphasized that Fig. 6 is the low AOA value of $K_{W(B)}$, and it gives no indication about how $K_{W(B)}$ will vary with AOA. As a result, some assumptions will be made. References 13 and 28 defined $K_{W(B)}$ and $K_{B(W)}$ as given in Eq. (13). As seen in Eq. (13), $K_{W(B)}$ has five parameters that are defined in tables as functions of wing aspect and taper ratio for various values of r/s, AOA, and M_∞. It will be assumed here that the results in Fig. 6 will be applied to the SBT value of $K_{W(B)}$ and $K_{B(W)}$ [that is, the first term of Eq. (13)]. As AOA increases, all of the parameters of the methods of Refs. 13 and 28 are then held constant except for the rate of change, $\mathrm{d}K_{W(B)}/\mathrm{d}\alpha$. In other words, at low-to-moderate AOA, the body cross section is allowed to change the interference factors from their circular body values, whereas at high AOA, it is not. Also, as a first approximation, the values of $\Delta K_{W(B)}$ and $\Delta K_{B(W)}$ available in the AP95 will be assumed to be independent of cross-sectional shape at AOA.

Figure 6 was based on fins located at a roll position of zero. References 13 and 28 have nonlinear treatment of fin carryover interference for both roll positions of 0 and 45 deg. As a result, the SBT results of Fig. 6 will be applied to the body with the fins in both the $\Phi = 0$ and 45 deg orientation. Of course, the nonlinearities with Mach number, AOA, and fin shape are different for these roll orientations and will be used as currently done in Refs. 13 and 28. As already stated, Eqs. (15–18) are used to compute $K_{B(W)}$, $k_{W(B)}$, and $k_{B(W)}$ for noncircular cross sections when the methods of Refs. 29 and 30 are used to compute $K_{W(B)}$ for the ellipse.

Reference 30 also presented results for $[K_{W(B)}]_{\alpha=0}$ for the triangular and square shapes. Two methods were used in that reference. For values of k between 0.125 and 0.5 and r/s between 0.167 and 0.667, a numerical code was used. To obtain the value of $K_{W(B)}$ for $r/s = 1.0$, the incompressible data of Ref. 17 were used in conjunction with the incompressible form of the Bernoulli equation.[30]

Following a procedure similar to that of Ref. 30, values of $K_{W(B)}$ for squares and triangles were obtained near AOA of 0 and for a limited number of values of corner radius. Using these values of $K_{W(B)}$ and engineering judgment to extrapolate in between values of k, Fig. 7 was derived for triangles and squares. Note that the wind-tunnel database of Fig. 7 was based on $A_{\text{ref}} = \pi W^2/4$ vs Fig. 6, which was based on $\pi d_{\text{eq}}^2/4$. The other interference factor terms for the squares and triangles are computed using Eqs. (15–18).

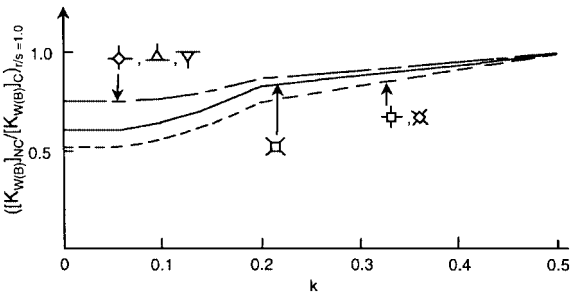

Fig. 7 Impact of square and triangular body cross sections on low Mach number values of $K_{W(B)}$ (data from Refs. 18 and 29 and based on $A_{\text{ref}} = \pi W^2/4$).

It is interesting to note that all of the interference factors in Fig. 7 are less than 1, compared with those in Fig. 6, which can be greater than 1. This apparent dilemma is created by the way the curves were drawn, i.e., Fig. 6 is based on $\pi d_{\text{eq}}^2/4$ and Fig. 7 on $\pi W^2/4$. This leads to a requirement for a scaling factor to relate one set of curves to another. The discussion of the slender body theory scaling factor that follows later in this paper elaborates on this issue.

Figure 7 gives values of $K_{W(B)}$ for squares and triangles at the limiting value of $r/s = 1$. Thus, to relate the value of $K_{W(B)}$ at some value of r/s other than 1 to Fig. 7, a linear assumption is used, similar to what occurs in SBT.[27] Hence,

$$\left[K_{W(B)}\right]_{\text{NC}} = \left\{\left[K_{W(B)}\right]_{\substack{\text{NC}\\ r/s=1}} - 1\right\}(r/s) + 1 \tag{19}$$

Using the value of $[K_{W(B)}]_{\text{NC}}$ computed from Eq. (19) for a given r/s, the nonlinear models of Refs. 13 and 28 are once again used to relate the wing–body aerodynamics as a function of AOA and Mach number. Equations (15–18) are used for the other interference terms, in analogy to the elliptical cross-sectional case.

G. Slender Body Theory Scaling Factor

In trying to develop a simple way to calculate the aerodynamics of noncircular wing–body configurations, there is an apparent scaling dilemma. The body aerodynamic calculations would appear to be more appropriately done based on a circle of equivalent cross-sectional area to the noncircular cross section. However, the wings would like to see a body of size equal to that of a circle of diameter W (see Fig. 7). This problem does not arise for bodies alone but only when wings are placed on the body. One could therefore calculate the aerodynamics of the wing body based on a circle of diameter W and then multiply the body aerodynamics by $A_{\text{eq}}/(\pi W^2/4)$ or calculate the aerodynamics based on a circular cylinder of diameter d_{eq} and multiply the wing aerodynamics by another scaling parameter defined in Ref. 14. The latter approach is chosen for the squares and triangles, and so a consistent approach for body alone aerodynamics is obtained with the ellipses.

In trying to understand this scaling factor, resort is made to SBT. Using SBT, one can rigorously show that there is a factor of $A_{\text{eq}}/(\pi W^2/4)$ between the equivalent circular case and a square or triangle if the square or triangle is represented by a circular cylinder of diameter W vs d_{eq}. Likewise if the diameter d_{eq} is used for the triangle or square as opposed to W, one can rigorously show there is a factor that multiplies the wing–body and body–wing contributions for low AOA. This factor is a function of r/s and wing area. Reference 14 gives a thorough discussion of scaling using SBT and its implications on calculating aerodynamics of configurations with noncircular cross-sectional bodies. The slender body scaling factors derived in Ref. 14 are required for use in computing aerodynamics of a nonaxisymmetric body with an axisymmetric body code.

H. Wing–Body–Tail Configurations

Wings and tails will be assumed to be in line at either roll positions of $\Phi = 0$ or 45 deg. This will allow the new wing–tail interference model developed and discussed in Ref. 28 to be used. Although this model will probably be impacted by noncircular shapes, it is believed that it is probably less of an impact than on either $K_{W(B)}$ or $K_{B(W)}$. There will be less impact because the vortices shed by the

wings are near the wing tips and, in most cases, are not impacted by the body cross-sectional shape. As a result of this assumption, the tail can be analyzed just as the wing, for the body cross section of interest at the tail. The only difference will be the addition of the downwash effect on the tail produced by the wing.

I. Variable Body Cross-Sectional Shapes

The discussion to this point has assumed a constant noncircular body cross-sectional shape. That is, the nose, afterbody, and boattail or flare all have the same cross-sectional shape. These shapes could be circular, elliptical, square, or triangular and oriented as shown in Fig. 1. In principle, the methodology for noncircular shaped missile configurations discussed in Secs. II.B–II.G for constant cross-sectional shape can be applied to configurations that have a variable cross section. To do this will require different values of the parameters $(C_n/C_{n0})_{SB}$, $(C_n/C_{n0})_N$, and NF and interference factors for each of the different cross-sectional shapes. From a practical hardware standpoint, only two different cross-sectional shapes will be allowed with a transition region between. For example, if the front of the missile were circular and the back elliptical, a transition region between circular and elliptical shape is necessary from a practical standpoint. It is necessary, therefore, to have a region that smoothly contours the nose ellipse to that of the afterbody. The cross-sectional area of this configuration remains constant from the end of the nose to the end of the body. This also means the equivalent diameter of a circular cross section also remains constant. However, the noncircular slender body and Newtonian factors are significantly different, which means the normal force, pitching moment, and center of pressure will change substantially.

III. Results and Discussion

The performance of the new nonaxisymmetric body methodology was evaluated[14] by applying it to an extensive array of aerodynamic configurations over a broad range of flight conditions. This included body alone configurations consisting of elliptical, square, and triangular cross sections. The elliptical configurations considered had a/b ratios varying from 0.5 to 2.0. Square, diamond, and triangular cross sections had corner roundness that varied between 0 and 0.33. Not all cases were available on all configurations, however. Freestream conditions varied from Mach numbers as low as 0.3 to as high as 14. AOAs as high as 60 deg were considered.

Several wing–body cases were also considered,[14] but not nearly as much data was available as for the body alone. Configuration geometry and flight conditions were more limited as well. Only one wing–body–tail case[14] was considered as this was the only case where data were found in the literature.

No average accuracy assessment has been made as of yet for the nonaxisymmetric body configurations similar to that available for axisymmetric bodies. As more comparisons are made, this may become more feasible. At present, the average accuracy of the normal and axial force coefficients and center of pressure appears to be almost as good as the axisymmetric body.

Only a sample of the Ref. 14 results will be shown here. All cases computed used an optimum value of the critical crossflow Mach number where transition from subcritical to supercritical conditions occur. This optimum value is not that critical for higher-Mach-number computations but is very important to accurately predict subsonic normal force. The first case considered is the configuration of Fig. 8. This configuration was tested to a 24-deg AOA at $M_\infty = 1.98$ and 3.88 in Ref. 7. All bodies in Fig. 8 have the same cross-sectional area as the circle. The corner radii of the squares and triangles were very small, and so a value of $k = 0$ was assumed in the computations. The elliptical shape 10-caliber body of Fig. 8 was tested later at Mach numbers 0.6–2.0 and to an AOA of 56 deg (Ref. 32). The case shown here will thus be the elliptical 10-caliber-long body tests of Ref. 32, which go to 56-deg AOA, and the square and triangular tests of Ref. 7, which go only to a 24-deg AOA. Not all results will be shown, as the Refs. 7 and 32 databases were fairly extensive. Most of these results are shown in Ref. 14, however.

Figures 9–11 give the elliptical body results for Mach numbers of 0.6, 1.2, and 2.0. Results shown are for ellipticity values of 0.5,

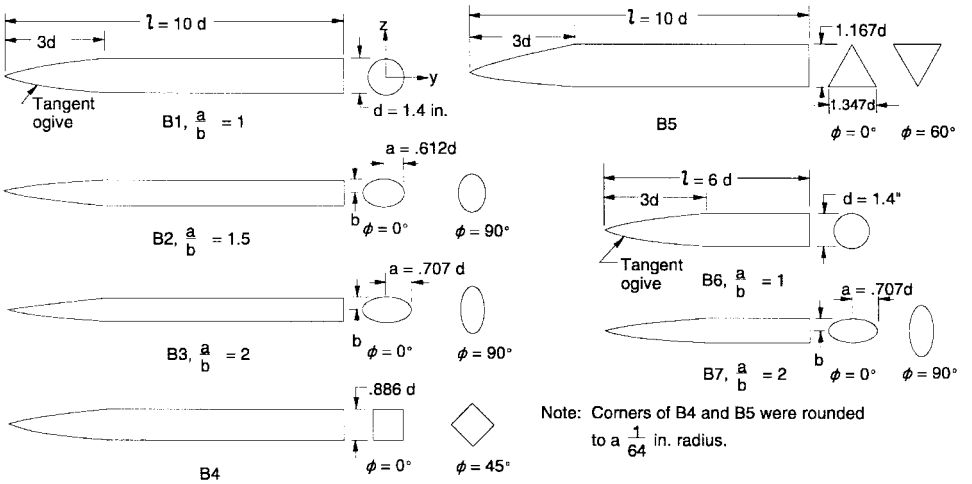

Fig. 8 Body alone configurations[7] with elliptical, square, diamond, triangular, and inverted triangular shapes.

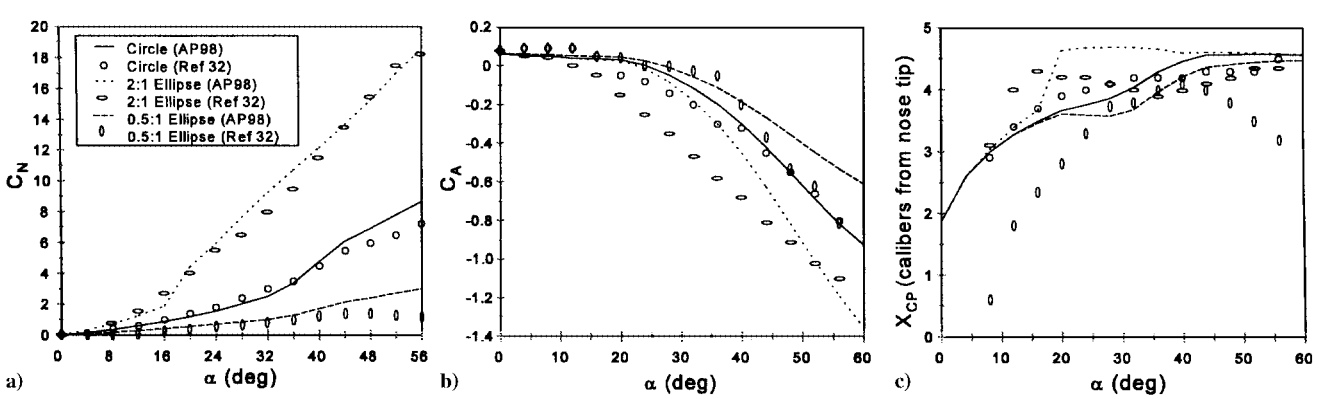

Fig. 9 Aerodynamic data for 2:1 and 0.5:1 ellipses of Fig. 8 compared with circular body at $M = 0.6$: a) normal force coefficient, b) axial force coefficient, and c) center of pressure.

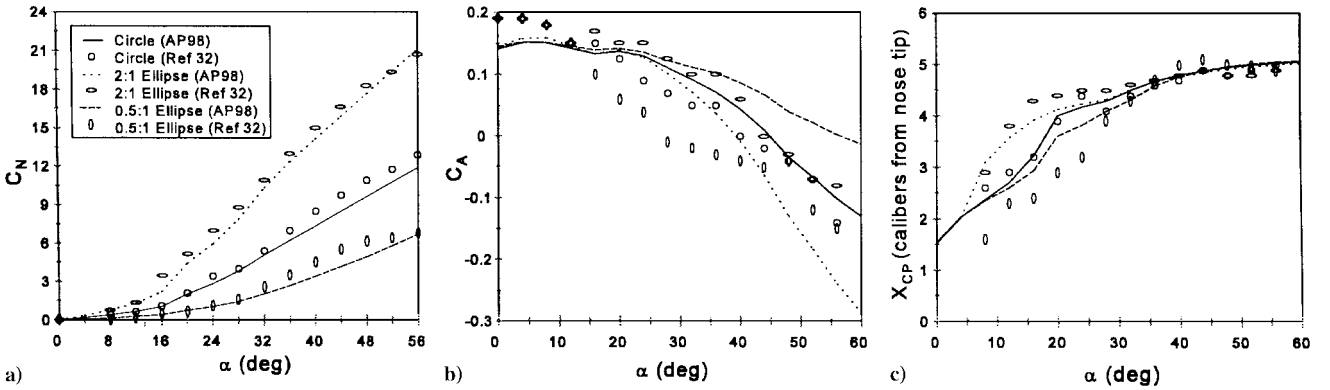

Fig. 10 Aerodynamic data for 2:1 and 0.5:1 ellipses of Fig. 8 compared with circular body at $M = 1.2$: a) normal force coefficient, b) axial force coefficient, and c) center of pressure.

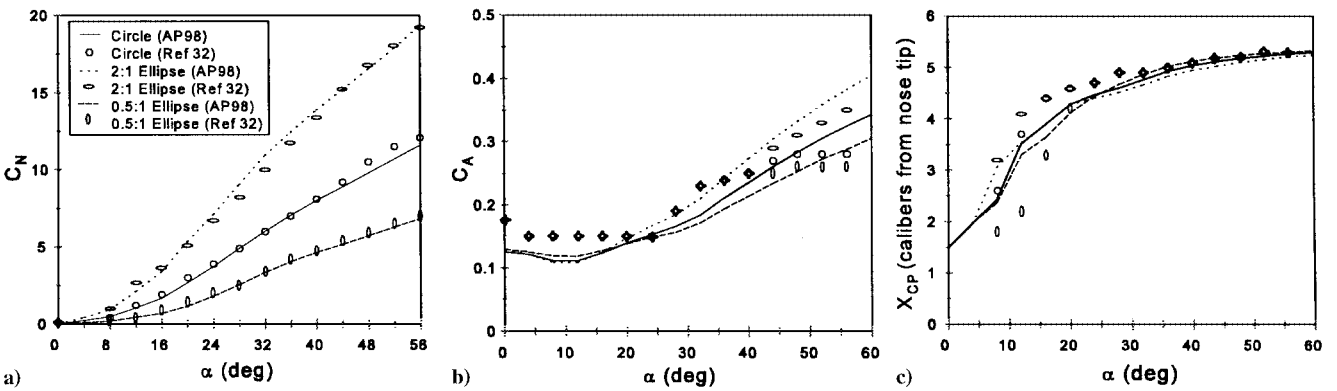

Fig. 11 Aerodynamic data for 2:1 and 0.5:1 ellipses of Fig. 8 compared with circular body at $M = 2.0$: a) normal force coefficient, b) axial force coefficient, and c) center of pressure.

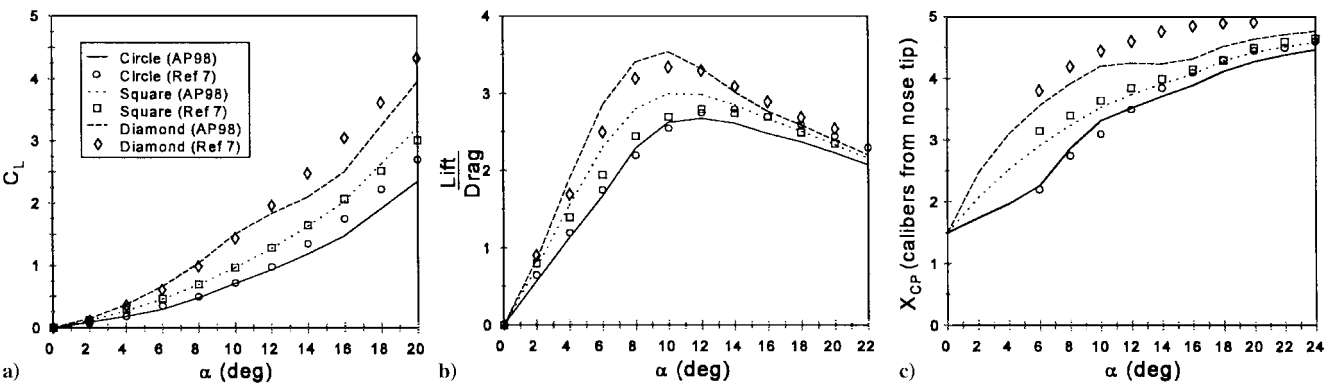

Fig. 12 Aerodynamic data of squares ($k = 0.0$) and diamonds ($k = 0.0$) of Fig. 8 compared with circular body at $M = 1.98$ ($l/d = 10$): a) lift coefficient, b) lift-to-drag ratio, and c) center of pressure.

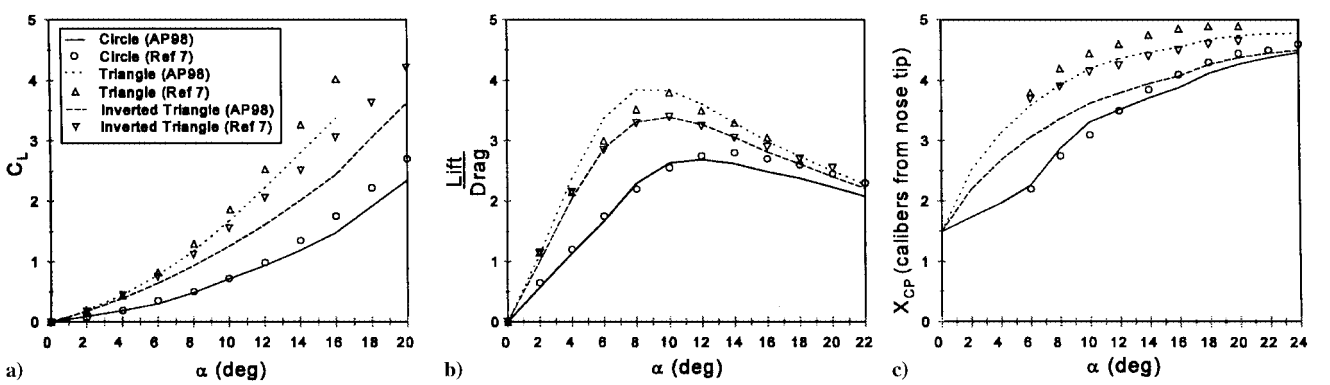

Fig. 13 Aerodynamic data of triangles ($k = 0.0$) and inverted triangles ($k = 0.0$) of Fig. 8 compared with circular body at $M = 1.98$ ($l/d = 10$): a) lift coefficient, b) lift-to-drag ratio, and c) center of pressure.

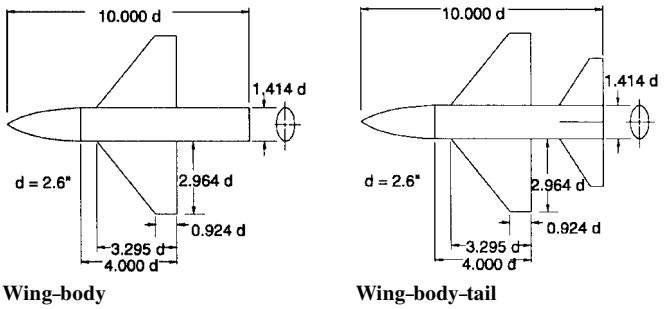

Fig. 14 Geometry of the wing–body and wing–body–tail configurations with 2:1 elliptical bodies.[6]

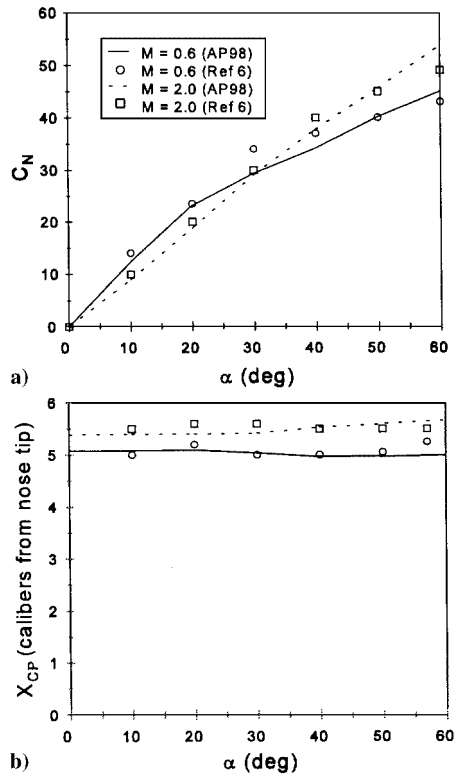

Fig. 15 Aerodynamic data for the wing–body configuration of Fig. 14 with a 2:1 elliptical cross-sectional body: a) normal force coefficient and b) center of pressure.

1.0, and 2.0 and are given in terms of normal and axial force coefficients and center of pressure. Also, the axial force coefficient does not include a base drag component. In examining the comparisons of theory and experiment in Figs. 9–11, it is seen that the theory does a fairly good job of predicting most of the aerodynamics on the $a/b = 2.0$ elliptical case at all three Mach numbers. The normal force and center of pressure predictions are quite encouraging as they are well within the average accuracy levels of ± 10 and $\pm 4\%$ of body length, respectively. The axial force prediction comparisons are not as good as desired. However, the poorer comparison of theoretical axial force to data could be due to measurement accuracy where it is difficult to get accurate axial force measurements with a sting designed for measuring normal force at high AOA. The $a/b = 0.5$ results are not quite as good as the $a/b = 2.0$ results, particularly at high AOA. This could be due to the critical value of crossflow Mach number prediction. The data appear to support supercritical flow up to an AOA of 56 deg, whereas the theory indicates the flow transitions to subcritical conditions around an AOA of 36–40 deg. Also the center of pressure prediction for the $a/b = 0.5$ case at low AOA appears to indicate a center of pressure much farther toward the nose tip at $M = 0.6$ than the theory predicts. It is not clear what mechanism causes this. Because the nose length is 3 calibers and there is no boat tail

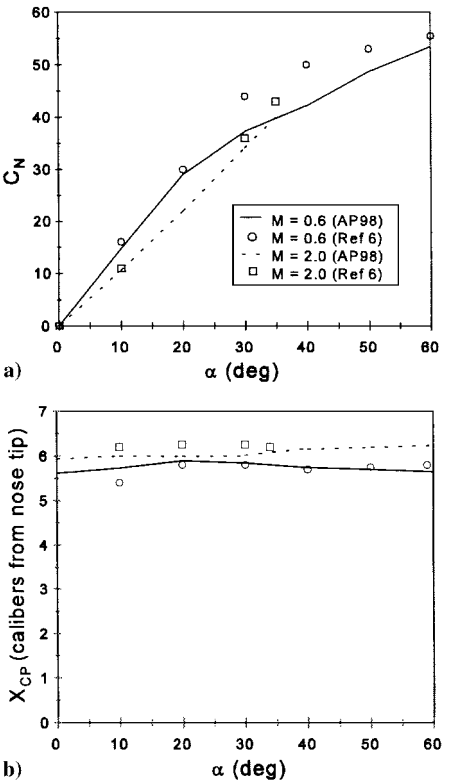

Fig. 16 Aerodynamic data for the wing–body–tail configuration of Fig. 14 with a 2:1 elliptical cross-sectional body: a) normal force coefficient and b) center of pressure.

present, intuition would lead one to expect the center of pressure to lie somewhere between 1.5 and 3.0 calibers from the nost tip near $\alpha = 0$ deg.

Theoretical and experimental results for the squares and triangles of Fig. 8 are given in Figs. 12 and 13, respectively. Only the 10-caliber-long configuration results at $M = 1.98$ are shown. Here the results are given in terms of lift coefficient, lift-to-drag ratio, and center of pressure. In general, comparison of theory and experiment for the squares and diamonds is quite encouraging, although not as good as the circular cross-sectional shapes. The triangular shaped body predictions for lift coefficient tend to be somewhat low as AOA increases. However, this is to be expected because the values for the circular cylinder results are also low. Lift-to-drag ratio predictions are quite good, with the peak values being reasonably well predicted. Center of pressure prediction for the triangular shape is well within the $\pm 4\%$ of body length used as a criterion for axisymmetric bodies. However, the inverted triangle center of pressure predictions slightly exceed this value.

The next case considered is a 10-caliber wing–body and wing–body–tail case shown in Fig. 14 (Ref. 6). The body cross section is an ellipse with an $a/b = 2.0$, and the nose length is 3.0 calibers. Figures 15 and 16 present the normal force and center of pressure comparisons of experiment and theory at $M = 0.6$ and 2.0 for the wing–body and wing–body–tail cases, respectively. Data for the wing–body–tail case at $M = 2.0$ were available only at $\alpha = 34$ deg, whereas all other cases have data to an AOA of 60 deg. As seen in Figs. 15 and 16, theoretical predictions are quite good for center of pressure and fair to good for normal force coefficient.

The third configuration shown (see Fig. 17) is a waverider configuration taken from Ref. 33. Lift, drag, and pitching moment comparisons of theory and experiment at $M = 14.0$ to $\alpha = 25$ deg are shown in Fig. 18. Results are quite encouraging, even though this configuration does not quite fit the triangular shape, which has 60-deg angles in all corners. Note that these results are based on a 375-in.^{2} planform area.

The final configuration considered, taken from Ref. 34, is shown in Fig. 19. It consists of a lifting body with variable sweep wing panels. In this case, we have a body that appears at first glance to

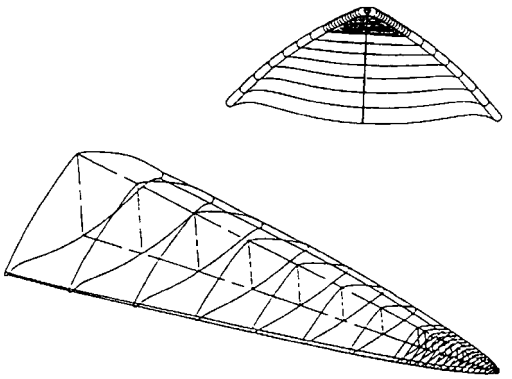

Fig. 17 Wire frame geometry of the waverider (adapted from Ref. 33).

be an inverted triangle, but the lower angle is only 45 deg and not 60 deg. In this sense, it resembles the lower half of a diamond. For comparison purposes, it was decided to run this example as both an inverted triangle and a diamond, both with sharp corners because the top corners were thought to be more influential on the flowfield. The wing panels were modeled at a 40-deg leading-edge sweep. Computations were performed for Mach numbers of 0.4, 0.6, and 0.8 with corresponding Reynolds numbers based on the maximum body chord of 5.04×10^6, 7.2×10^6, and 9.36×10^6, respectively. The lift coefficients for the wind-tunnel tests and the AP98 computations for both body shapes are shown for the three Mach numbers in Fig. 20. The coefficient values shown are based on the planform area of the body (96.2 in.^{2}). On balance, both approaches give acceptable results, with the diamond being somewhat better in most cases. The diamond may give these good results because it more closely represents the true angle on the body's lower

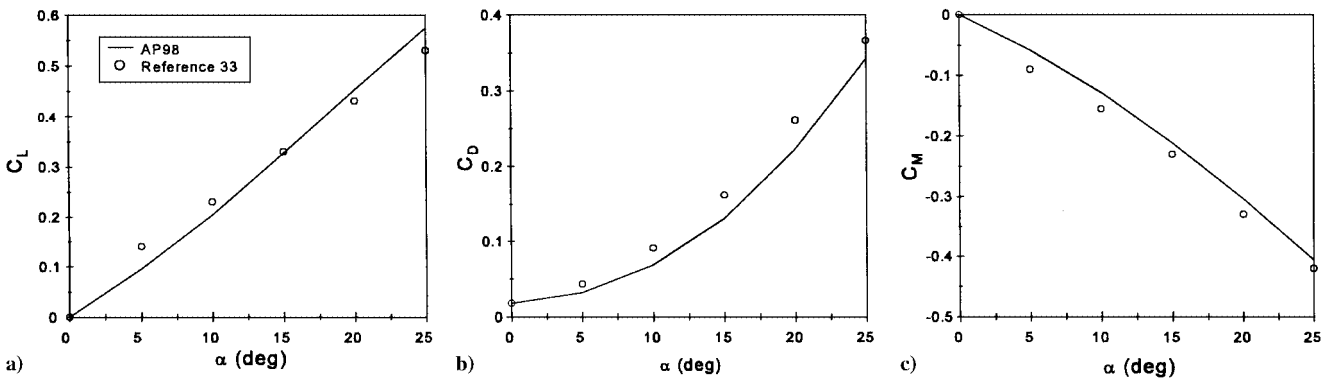

Fig. 18 Aerodynamic data for the Mach 14 waverider of Fig. 17: a) lift coefficient, b) axial force coefficient, and c) moment coefficient.

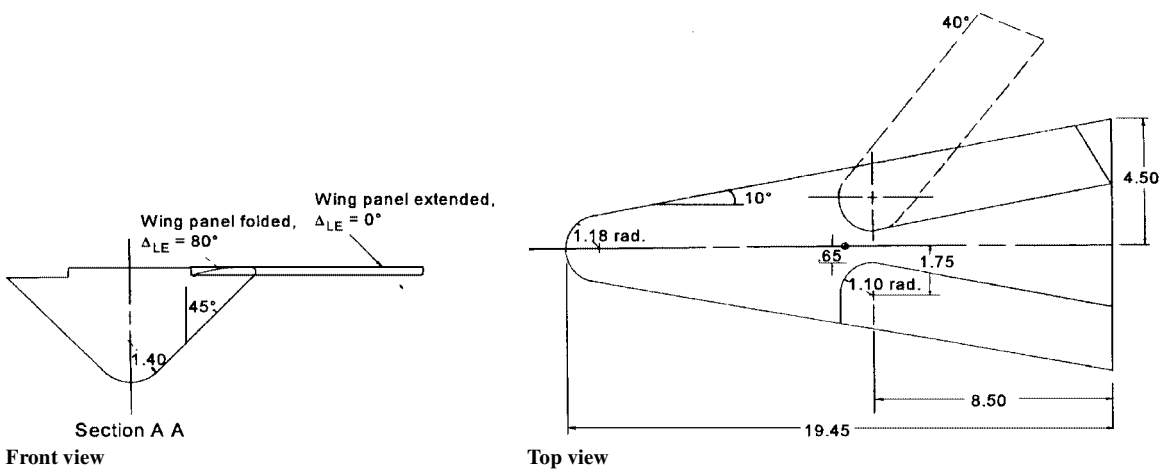

Fig. 19 Geometry of the variable wing sweep lifting body (from Ref. 34).

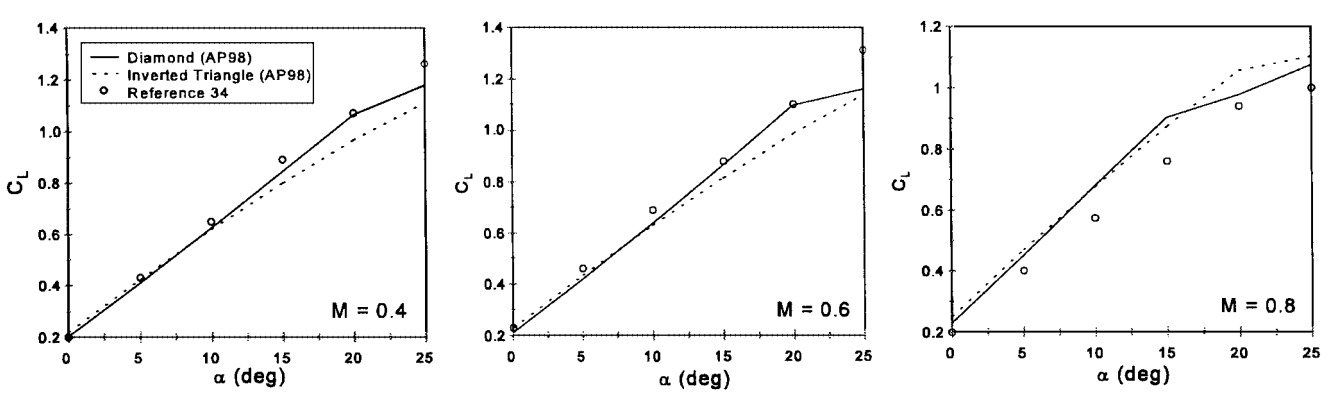

Fig. 20 Lift coefficients for the body–wing configuration of Fig. 19 computed by two methods and at three Mach numbers.

surface, and it is the windward side aerodynamics that dominate the flowfield.

IV. Conclusions

An improved method has been developed to compute aerodynamics of noncircular cross-sectional shapes. The improved method is based on the Jorgensen approach of computing aerodynamics on a noncircular body using circular body methods, on the Nelson approach for noncircular wing–body interference corrections at low AOA, and on the method of the present authors for including nonlinearities in the wing–body interference aerodynamics. The new method extends these approaches in several significant ways so as to make the method more general and applicable to most configurations of noncircular cross section.

Specific additions to the current state of the art include derivation of the Newtonian approximation to the local normal force coefficient per unit length of a noncircular shape to the similar coefficient of a circular shape; derivation of an empirical correction to these Newtonian factors to account for the assumption of a high Mach number in their derivation; derivation of an empirical estimate of critical crossflow Reynolds number as a function of the noncircular geometry shape; a method to treat wing–body interference factor corrections as a function of body geometry and freestream parameters; derivation of slender body theory scaling factors to allow aerodynamics to be computed and compared with wind-tunnel data where the equivalent diameter or a diameter equal to the side of a square or triangle is used in the data gathering; and an approximate way of treating configurations that have variable, noncircular cross-sectional shapes.

The new method was applied to all of the noncircular configurations found in the literature for which data were available. This included elliptical cross-sectional shapes with a/b from 0.5 to 3.0, Mach numbers from 0.6 to 3.88, and AOA as high as 58 deg, and some cases with wings; square and triangular cross-sectional shapes with sharp and rounded edges, at mostly lower Mach numbers, but some data at Mach numbers as high as 4, AOA as high as 58 deg, and some cases with wings; a single configuration with a variable cross-sectional shape at Mach numbers from 0.6 to 2.0 and AOA to 60 deg; and to two configurations that were quite complex and did not fit within the exact requirements of the geometry options. Results in general for planar aerodynamics using a semiempirical code were very good. Although it is too early to state the overall accuracy of the new nonaxisymmetric body aerodynamic prediction method, it appears that the normal force is almost as good as the circular body predictions. To date, we have not found a circular body configuration where average accuracy on C_A and C_N exceeds $\pm 10\%$ and X_{CP} exceeds $\pm 4\%$ of the body length. Here "average" means enough Mach numbers and AOAs to get a good statistical sample.

Although the additions to the state of the art in computing approximate aerodynamics are significant, several challenges remain. The first and foremost is to compare the present predictions of static aerodynamics to more data. Because many databases shown in the literature focus on normal force, additional data or computational fluid dynamics computations may be needed to validate and/or modify the axial force and center of pressure prediction techniques. It is hoped that the ballistics range tests at Eglin Air Force Base will partially address this problem for axial force and low AOA center of pressure prediction. Second, it is suspected that once more zero angle-of-attack axial force data are available, the assumption of the wave drag on the nonaxisymmetric body being equal to that of the axisymmetric body may need to be adjusted. Finally, it is suspected that the Newtonian correction factor for triangles and squares could be improved upon with more data or computational fluid dynamics computations.

Acknowledgments

The work described in this paper was supported through the Office of Naval Research (Dave Siegel) by the following programs: the Air Launched Weapons Program managed at the Naval Air Warfare Center, China Lake, California, by Tom Loftus and Craig Porter, and the Surface Weapons Systems Technology Program managed at the Naval Surface Warfare Center, Dahlgren Division, by Robin Staton and Gil Graff. Also, some support was provided by the Marine Corps Weaponry Technology Program managed at the Naval Surface Warfare Center, Dahlgren Division, by Bob Stiegler. The authors express appreciation for support received in this work.

References

[1]Gentry, A. E., Smyth, D. N., and Oliver, W. R., "The Mark IV Supersonic-Hypersonic Arbitrary Body Program," U.S. Air Force Flight Dynamics Lab., AFFDL TR-73-159, Wright–Patterson AFB, Dayton, OH, 1973.

[2]Sidwell, K. W., Baruah, P. K., and Bussoletti, J. E., "A Computer Program for Predicting Subsonic or Supersonic Linear Potential Flows About Arbitrary Configurations Using a Higher Order Panel Method," NASA CR-3252, Vol. 2, 1980.

[3]Wardlaw, A. B., and Davis, S., "A Second-Order-Gudonov Method for Supersonic Tactical Missiles," U.S. Naval Surface Warfare Center, Dahlgren Div., NSWC TR-86-506, Dahlgren, VA, Nov. 1986.

[4]Walters, R. W., Slack, D. C., Cimmella, P., Applebaum, M. P., and Frost, C., "A Users Guide for GASP," Aerosoft, Inc., Blacksburg, VA, Nov. 1990.

[5]Whitcomb, R. T., "A Study of the Zero-Lift Drag Rise Characteristics of Wing–Body Combinations Near the Speed of Sound," NACA Rept. 1273, 1956.

[6]Jorgensen, L. H., "Prediction of Static Aerodynamic Characteristics for Slender Bodies Alone and with Lifting Surfaces to Very High Angles of Attack," NASA TR-R-474, Sept. 1977.

[7]Jorgensen, L. H., "Inclined Bodies of Various Cross Sections at Supersonic Speeds," NASA Memo 10-3-58A, 1958.

[8]Jorgensen, L. H., "Prediction of Static Aerodynamic Characteristics for Space-Shuttle-Like and Other Bodies at Angles of Attack from 0° to 180°," NASA TN-D-6996, Jan. 1973.

[9]Jorgensen, L. H., "Estimation of Aerodynamics for Slender Bodies Alone and with Lifting Surfaces at α's from 0° to 90°," *AIAA Journal*, Vol. 11, No. 3, 1973, pp. 409–412.

[10]Jorgensen, L. H., "A Method for Estimating Static Aerodynamic Characteristics for Slender Bodies of Circular and Noncircular Cross Section Alone and with Lifting Surfaces at Angles of Attack from 0° to 90°," NASA TN-D-7228, April 1973.

[11]Vukelich, S. R., Stoy, S. L., Burns, K. A., Castillo, J. A., and Moore, M. E., "'Missile DATCOM'—Volume I—Final Report," U.S. Air Force Wright Aeronautical Labs., AFWAL-TR-86-3091, Wright–Patterson AFB, OH, Dec. 1988.

[12]Hemsch, M. J., and Nielsen, J. N., "Equivalent Angle-of-Attack Method for Estimating Nonlinear Aerodynamics of Missile Fins," *Journal of Spacecraft and Rockets*, Vol. 20, No. 4, 1983, pp. 356–362.

[13]Moore, F. G., McInville, R. M., and Hymer, T., "The 1995 Version of the NSWC Aeroprediction Code: Part I—Summary of New Theoretical Methodology," U.S. Naval Surface Warfare Center, Dahlgren Div., NSWCDD/TR-94/379, Dahlgren, VA, Feb. 1995.

[14]Moore, F. G., McInville, R. M., and Hymer, T. C., "An Improved Semiempirical Method for Calculating Aerodynamics of Missiles with Noncircular Bodies," U.S. Naval Surface Warfare Center, Dahlgren Div., NSWCDD/TR-97/20, Dahlgren, VA, Sept. 1997.

[15]Moore, F. G., and Hymer, T. C., "An Improved Method for Predicting Axial Force at High Angle of Attack," U.S. Naval Surface Warfare Center, Dahlgren Div., NSWCDD/TR-96/240, Dahlgren, VA, Feb. 1997.

[16]Jones, N. H., and Zollars, G. J., "Investigation of the Aerodynamics of Square Cross Section Missiles," U.S. Air Force Academy, USAFA-TR-83-15, Colorado Springs, CO, Sept. 1983.

[17]Polhamus, E. C., Geller, B. W., and Greenwald, K. J., "Pressure and Force Characteristics of Noncircular Cylinders as Affected by Reynolds Number with a Method Included for Determining the Potential Flow About Arbitrary Shapes," NASA TR-R-46, 1959.

[18]Lockwood, V. E., "Effects of Reynolds Number and Flow Incidence on the Force Characteristics of a Family of Flat-Front Cylinders," NASA TN-D-3932, May 1967.

[19]Polhamus, E. C., "Effect of Flow Incidence and Reynolds Number on Low-Speed Aerodynamic Characteristics of Several Noncircular Cylinders with Applications to Directional Stability and Spinning," NACA TN-4176, Jan. 1958.

[20]Daniel, D. C., Yechout, T. R., and Zollars, G. J., "Experimental Aerodynamic Characteristics of Missiles with Square Cross Sections," *Journal of Spacecraft and Rockets*, Vol. 19, No. 2, 1982, pp. 167–172.

[21]Schneider, W., "Experimental Investigation of Bodies with Noncircular Cross Section in Compressible Flow," CP-336, AGARD, Sept. 1982, pp. 19-1–19-15.

[22]Sellers, M. E., and Siler, L. G., "Pressure and Static Force Test of Three Elliptic Missile Body Configurations at Mach Numbers 1.5 to 5.0," Arnold Engineering Development Center, AEDC-TSR-83-V44, Tullahoma, TN, 1983.

[23]Shereda, D. E., Amidon, P. F., Dahlem, V., III, and Brown-Edwards, E., "Pressure Test of Three Elliptical Missile Body Configurations at Mach Numbers 1.5 to 5.0," U.S. Air Force Wright Aeronautical Labs., AFWAL TM 84-236-FIMG, Wright–Patterson AFB, OH, Dec. 1984.

[24]Lijewski, L. E., Zollars, G. J., Yechout, T. R., and Haupt, B. F., "Experimental Flowfield Measurements of Missiles with Square Cross Sections," AIAA Paper 82-0055, Jan. 1982.

[25]Stoy, S. L., and Vukelich, S. R., "Prediction of Aerodynamic Characteristics of Unconventional Missile Configurations Using Component Buildup Techniques," AIAA Paper 86-0489, Jan. 1986.

[26]Delany, N. K., and Sorensen, N. E., "Low Speed Drag of Cylinders of Various Shapes," NACA TN-3038, Nov. 1953.

[27]Pitts, W. C., Nielsen, J. N., and Kaattari, G. E., "Lift and Center of Pressure of Wing-Body-Tail Combinations at Subsonic, Transonic, and Supersonic Speeds," NACA TR-1307, 1957.

[28]Moore, F. G., and McInville, R., "Extension of the NSWCDD Aeroprediction Code to the Roll Position of 45 Degrees," U.S. Naval Surface Warfare Center, Dahlgren Div., NSWCDD/TR-95/160, Dahlgren, VA, Dec. 1995.

[29]Nelson, H. F., "Wing-Body Interference Lift for Supersonic Missiles with Elliptical Cross-Section Fuselages," *Journal of Spacecraft and Rockets*, Vol. 26, No. 5, 1989, pp. 322–329.

[30]Est, B. E., and Nelson, H. F., "Wing-Body Carryover and Fin Center of Pressure for Missiles with Noncircular Fuselage Cross Sections," AIAA Paper 91-2856, Aug. 1991.

[31]Sigal, A., "Methods of Analysis and Experiments for Missiles with Noncircular Fuselages," *Tactical Missile Aerodynamics*, edited by J. Nielsen, Progress in Aeronautics and Astronautics, AIAA, Washington, DC, 1991, pp. 171–217.

[32]Jorgenson, L. H., and Nelson, E. R., "Experimental Aerodynamic Characteristics for Bodies of Elliptic Cross Section at Angles of Attack from 0° to 58° and Mach Numbers from 0.6 to 2.0," NASA TM-X-3129, 1975.

[33]Gillum, M. J., and Lewis, M. J., "Analysis of Experimental Results on a Mach 14 Waverider with Blunt Leading Edges," AIAA Paper 96-0812, Jan. 1996.

[34]Spencer, B., "Longitudinal Aerodynamic Characteristics at Mach Numbers from 0.40 to 1.10 of a Blunted Right-Triangular Pyramidal Lifting Reentry Configuration Employing Variable-Sweep Wing Panels," NASA TN-D-1518, 1963.

R. M. Cummings
Associate Editor